Ceramics International xxx (xxxx) xxx

Contents lists available at ScienceDirect

Ceramics International

journal homepage: www.elsevier.com/locate/ceramint

Microwave dielectric properties of silico-carnotite $Ca_3M_2Si_3O_{12}$ (M= Yb, Y) ceramics synthesized via high energy ball milling

Yu Wang [a,c], Ying Tang [a,b,*], Jie Li [a,b,**], Weishuang Fang [a], Shiyao Shen [a], Feihu Li [a], Lian Duan [a], Ming Qin [c], Liang Fang [a,c,***]

[a] Guangxi Key Laboratory of Optical and Electronic Materials and Devices, College of Material Science and Engineering, Guilin University of Technology, Guilin, 541004, China

[b] Key Laboratory of Nonferrous Materials and New Processing Technology, Ministry of Education, Guilin University of Technology, Guilin, 541004, PR China

[c] College of Material Science and Engineering, Baise University, Baise, 533000, China

ARTICLE INFO

Keywords:
Microwave dielectric ceramic
High energy ball mill
Low permittivity
Infrared reflectivity

ABSTRACT

The $Ca_3M_2Si_3O_{12}$ (M = Yb, Y) ceramics with orthorhombic silico-carnotite structure were fabricated via high-energy ball milling and solid-state reaction route. Dense $Ca_3Yb_2Si_3O_{12}$ and $Ca_3Y_2Si_3O_{12}$ ceramics sintered at 1260 °C and 1240 °C revealed promising microwave dielectric properties with ε_r = 9.2 and 8.7, $Q\times f$ = 56,400 GHz and 29,094 GHz, τ_f = −77.5 ppm/°C and −76.8 ppm/°C, respectively. The connection between crystal structure and $Q\times f$ values of $Ca_3M_2Si_3O_{12}$ (M = Yb, Y) ceramics was discussed with respect to the packing fraction, and their intrinsic microwave dielectric properties were examined using the infrared reflectivity spectra analysis. The thermal stability of $Ca_3Yb_2Si_3O_{12}$ was improved successfully by forming $0.91Ca_3Yb_2Si_3O_{12}$-$0.09CaTiO_3$ composite ceramics with τ_f = +2.9 ppm/°C, ε_r = 12.93 and $Q\times f$ = 26,729 GHz.

1. Introduction

For several years, microwave dielectric ceramics occupy an unshakable position in the applications of dielectric resonators, filters, substrates, capacitors and oscillators, which have become an indispensable part of our digitized life. With the development of modern communication systems, faster transmission speed and higher quality of signals are required, resulting in the urgent need for high-quality and low-cost microwave dielectric ceramics [1]. Therefore, the performance requirements on ceramics are mainly divided into the following aspects: (1) high quality factor ($Q \times f$); (2) low permittivity (ε_r); (3) near-zero temperature coefficient of resonance frequency (τ_f), satisfying the requirements of excellent frequency selectivity, high speed of electronic signal transition and good thermal stability, respectively [2,3].

Recently, the garnet family with the general formula of $A_3B_2C_3O_{12}$ exhibit the characteristics of low permittivity and high performances, such as $Ca_3Y_2Ge_3O_{12}$, $Mg_3Y_2Ge_3O_{12}$, $Ca_3Al_2Ge_3O_{12}$, $AgCa_2Zn_2V_3O_{12}$, $AgCa_2Mg_2V_3O_{12}$ [4–6]. $Ca_3Y_2Si_3O_{12}$, which agrees with the general chemical formula of the garnet-structure $A_3B_2C_3O_{12}$, while, it was reported as the orthorhombic silico-carnotite structure by D.L. Poerschke and H. Yamane [7,8]. The crystal structure of silicate compounds with the stoichiometric of $Ca_3M_2Si_3O_{12}$ depends mainly on the Ionic radius of M. Silicon-based garnets based on Ca^{2+} ion are generally stable when the ionic radius of M is less than 0.8 Å. And for the cation with a larger radius, like Y^{3+} (0.892 Å) and Lu^{3+} (0.848 Å), they cannot form the octahedron in garnet under the environment of six coordination. It is therefore unlikely to be a garnet structure [9]. The visible luminescence of lanthanide ions, spectroscopic characterization, photoluminescence properties and effects of doping with Ce^{3+}, Tb^{3+} and Sm^{3+} on luminescent properties of $Ca_3Y_2Si_3O_{12}$ were researched [9–12]. To our knowledge, the microwave dielectric properties of $Ca_3Y_2Si_3O_{12}$ ceramics have not been explored yet. Besides, Poerschke reported that the calcium-silicon-yttrium systems had a high synthesis temperature (1500 °C), which increased the cost of material production and

* Corresponding author. Guangxi Key Laboratory of Optical and Electronic Materials and Devices, College of Material Science and Engineering, Guilin University of Technology, Guilin, 541004, China.

** Corresponding author. Guangxi Key Laboratory of Optical and Electronic Materials and Devices, College of Material Science and Engineering, Guilin University of Technology, Guilin, 541004, China.

*** Corresponding author. Guangxi Key Laboratory of Optical and Electronic Materials and Devices, College of Material Science and Engineering, Guilin University of Technology, Guilin, 541004, China.

E-mail addresses: tangyinggl001@aliyun.com (Y. Tang), jielee2019@aliyun.com (J. Li), fanglianggl001@aliyun.com (L. Fang).

https://doi.org/10.1016/j.ceramint.2020.10.054
Received 12 August 2020; Received in revised form 18 September 2020; Accepted 8 October 2020
Available online 9 October 2020

consumption [9]. Lin et al. obtained pure phase and dense Mg_2SiO_4 ceramics at 1075 °C by high-energy ball milling (HEBM), and reduced the sintering temperature by 300 °C [13,14]. This synthetic method is beneficial to improving the reaction rate and densification of ceramics [15].

In this paper, we prepared $Ca_3M_2Si_3O_{12}$ (M = Yb, Y) ceramics by HEBM and the solid-state reaction method, due to the similar ion radius of Yb^{3+} (0.868 Å) compared with Y^{3+} (0.892 Å) [16]. The grain morphology, and microwave dielectric properties as well as infrared reflectivity spectra were studied systematically.

2. Experimental procedure

The $CaCO_3$, SiO_2, Yb_2O_3, and Y_2O_3 with the purity of 99.99% made by Aladdin were used as raw materials to prepare $Ca_3M_2Si_3O_{12}$ (M = Yb, Y) ceramics through the solid-state reaction method. The Yb_2O_3 or Y_2O_3 powders were dried at 900 °C for 2 h to avoid the absorption of moisture before weighting. The $Ca_3M_2Si_3O_{12}$ (M = Yb, Y) powders were weighed and mixed thoroughly via HEBM at a rate of 300 r/min in ethanol for 8 h. Then the slurries were desiccative at 120 °C, pressed uniaxially and heated to 1100 °C for 6 h at a rate of 5 °C/min. The calcined samples were then ground into fine powders, and pressed into pellets (10 mm × 6 mm) under 200 MPa with 5 wt% PVA as a binder and fired at 1180–1260 °C for 12 h to achieve the dense ceramics.

The particle size analysis was performed by a Nanopartide and Zeta potential Analyzer. The phase purity and the date of Rietveld refinements were collected by an X-ray diffractometer. The apparent bulk density of samples was obtained by Archimedes method. The surface microstructure of the $Ca_3M_2Si_3O_{12}$ (M = Yb, Y) ceramics were observed by scanning electron microscopy. The ε_r and $Q\times f$ of ceramic samples were measured by the Hakki-Coleman parallel plate method based on network analyzer. The temperature coefficient of resonant frequency (τ_f) was measured in the range of 25–85 °C.

The analysis of the Infrared reflectivity spectra of the $Ca_3M_2Si_3O_{12}$ (M = Yb, Y) ceramics was conducted using the infrared beamline station at National Synchrotron Radiation Lab. (NSRL, China), by Bruker IFS 66v FTIR spectrometer. The complex dielectric response was analyzed for the infrared spectra according to the harmonic oscillator model, and the formula is as follows [17]:

$$\varepsilon^*(\omega) = \varepsilon_\infty + \sum_{j=1}^{n} \frac{\omega_{pj}^2}{\omega_{oj}^2 - \omega^2 - j\gamma_j\omega} \quad (1)$$

where $\varepsilon^*(\omega)$ refers to the complex permittivity and ε_∞ refers to the permittivity at high frequency electronic polarization. The γ_j, ω_{oj}, and ω_{pj} represent the decay factor, the transverse frequency, and the plasma frequency of the j-th Lorenz oscillator, respectively, and n is the number of transverse phonon modes. The reflectivity $R(\omega)$ can be written as [18]:

$$R\left(\omega\right) = \left|\frac{1-\sqrt{\varepsilon^*(\omega)}}{1+\sqrt{\varepsilon^*(\omega)}}\right|^2 \quad (2)$$

3. Results and discussions

Fig. 1 manifests the particle size distribution and SEM of the mixed powders of $CaCO_3$, Yb_2O_3, and SiO_2 after conventional ball milling (Fig. 1 (a), (c)) and HEBM method (Fig. 1 (b), (d)), respectively. The agglomeration of the powders by traditional ball milling is obvious, with an average size of 642 nm. Noteworthily, the particle distribution of the powders after high-energy ball milling for 8 h is uniform, with a small average size of 297 nm, which is beneficial for accelerating sintering process and reducing the sintering temperature [13–15]. In this study, the high-energy ball milling method was chosen to prepare the $Ca_3M_2Si_3O_{12}$ (M = Yb, Y) ceramics.

Fig. 2 shows the XRD patterns of $Ca_3M_2Si_3O_{12}$ (M = Yb, Y) ceramics sintered at 1240 °C and 1260 °C for 12 h, respectively. For both specimenhttp://dict.youdao.com/w/eng/specimen/javascript:void(0);s, all

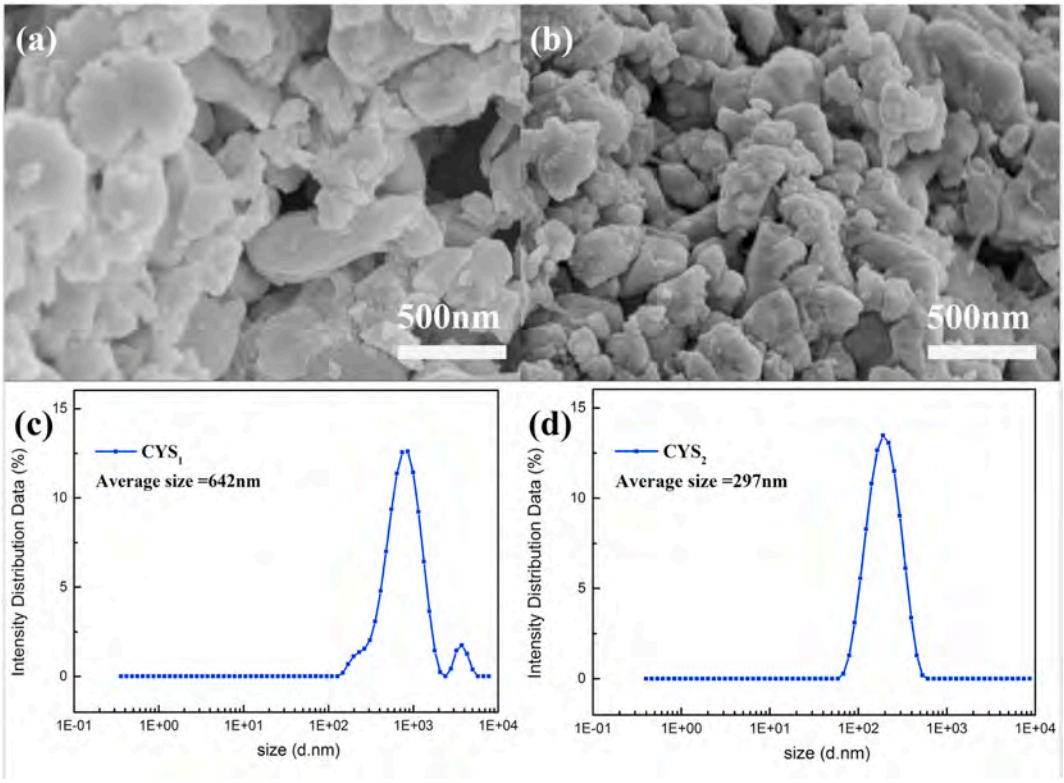

Fig. 1. The particle size distribution and SEM of the mixed powders of $CaCO_3$, Yb_2O_3, and SiO_2 after conventional ball milling (a), (c) and high-energy ball milling (b), (d).

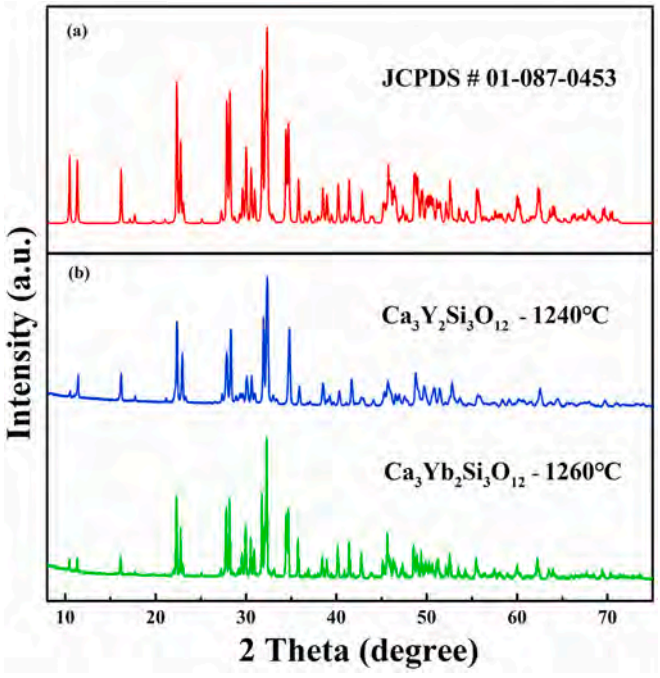

Fig. 2. XRD patterns of $Ca_3M_2Si_3O_{12}$ (M = Yb, Y) ceramics sintered at 1240 °C and 1260 °C for 12 h.

the observed diffraction peaks were in good agreement with $Ca_3Y_2Si_3O_{12}$ (JCPDS#01-087-0453) of the orthorhombic structure with a space group Pnma. No other peaks were observed, which showed the existence of a single-phase.

The Rietveld structure refinements were performed on the basis of the slow scanning XRD data of $Ca_3M_2Si_3O_{12}$ (M = Yb, Y) ceramics. The experimental data and refined XRD patterns for $Ca_3M_2Si_3O_{12}$ (M = Yb, Y) ceramics are showed in Fig. 3(a) and (b). The refined cell parameters were $a = 6.5483$ Å, $b = 15.4931$ Å, $c = 10.0035$ Å, $V = 1026.501$ Å^3 and $a = 6.54897$ Å, $b = 15.6160$ Å, $c = 10.0372$ Å, $V = 1014.842$ Å^3, with acceptable reliability factors of the profile $R_p = 5.7\%$, $R_{wp} = 8.2\%$ and $R_p = 9.8\%$, $R_{wp} = 12.9\%$ for $Ca_3Yb_2Si_3O_{12}$ and $Ca_3Y_2Si_3O_{12}$, respectively.

Fig. 4 shows the SEM micrographs of the $Ca_3M_2Si_3O_{12}$ (M = Yb, Y) ceramics. From Fig. 4 (a)–(e), it can be seen that, with the increment of temperature, the pores of $Ca_3Y_2Si_3O_{12}$ ceramics continuously decrease and the microstructure becomes relatively dense. The uniform grains of $Ca_3Y_2Si_3O_{12}$ ceramics were obtained at 1240 °C, with an average grain size of 1.6 μm. And an abnormal growth occurs as the temperature increases further to 1260 °C. The dense microstructure with a clear grain boundary is observed in Fig. 4 (f) for the $Ca_3Yb_2Si_3O_{12}$ sintered at 1260 °C, with an average grain size of 1.32 μm.

The dependence of relative density of the $Ca_3M_2Si_3O_{12}$ (M = Yb, Y) ceramics on sintering temperature is presented in Fig. 5(a). The relative density of $Ca_3M_2Si_3O_{12}$ (M = Yb, Y) ceramics was positively related to the sintering temperature, and it reached saturation at a certain temperature. The bulk density of samples reached a maximum value of ~4.78 g/cm^3 (98.36% of the theoretical density) for $Ca_3Yb_2Si_3O_{12}$ sintered at 1260 °C and ~3.52 g/cm^3 (94.6% of the theoretical density) for $Ca_3Y_2Si_3O_{12}$ sintered at 1240 °C. There was a slight decrease when the temperature was further increased, which might be caused by the abnormal grain growth. The change of ε_r as sintering temperature is presented in Fig. 5(b) ε_r increased firstly and then decreased slightly with the increase of temperature, reaching the maximum value of 9.2 for $Ca_3Yb_2Si_3O_{12}$ and 8.7 for $Ca_3Y_2Si_3O_{12}$, respectively. The permittivity is influenced by various factors, like relative density and ionic polarization [19]. The permittivity is mainly influenced by the ionic polarizabilities as to the single-phase samples with high relative densities (>95%). The Clausius–Mossotti equation can be applied to calculate the theoretical permittivity [20]:

$$\varepsilon_r = \frac{3V_m + 8\pi\alpha}{3V_m - 4\pi\alpha} \tag{3}$$

in which, V_m is the cell volume, α is the total amount of all ionic polarizability. α can be calculated by the following equation:

$$\alpha(Ca_3Y_2Si_3O_{12}) = 3\alpha(Ca^{2+}) + 2\alpha(Y^{3+}) + 3\alpha(Si^{4+}) + 12\alpha(O^{2-}) \tag{4}$$

where, $\alpha(Ca^{2+})$, $\alpha(Y^{3+})$, $\alpha(Si^{4+})$ and $\alpha(O^{2-})$,are 3.16 Å^3,3.81 Å^3,0.87 Å^3 and 2.01 Å^3, respectively [21]. The calculated theoretical permittivity is 8.5278 for $Ca_3Yb_2Si_3O_{12}$ and 8.55 for $Ca_3Y_2Si_3O_{12}$. The relative error of $Ca_3Yb_2Si_3O_{12}$ between the measured permittivity and the theoretical value is 7.9%, and 1.7% for $Ca_3Y_2Si_3O_{12}$, indicating the presence of rattling cations in $Ca_3Yb_2Si_3O_{12}$ [4].

Fig. 6 presents the variation in $Q\times f$ and τ_f values of $Ca_3M_2Si_3O_{12}$ (M = Yb, Y) ceramics. The variation tendency of the $Q\times f$ with sintering temperature was comparable to that of the permittivity and relative density. For the samples with the highest density, the optimal $Q\times f$

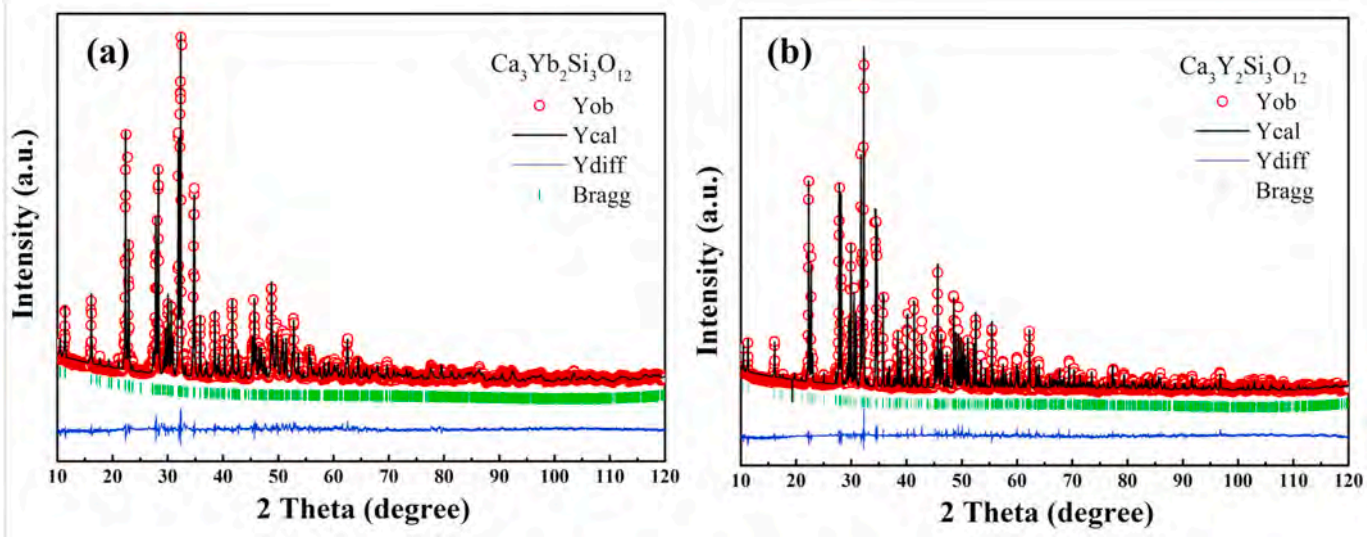

Fig. 3. The Rietveld refinement plots of $Ca_3M_2Si_3O_{12}$ (M = Yb, Y) ceramics sintered at 1260 °C and 1240 °C for 12 h.

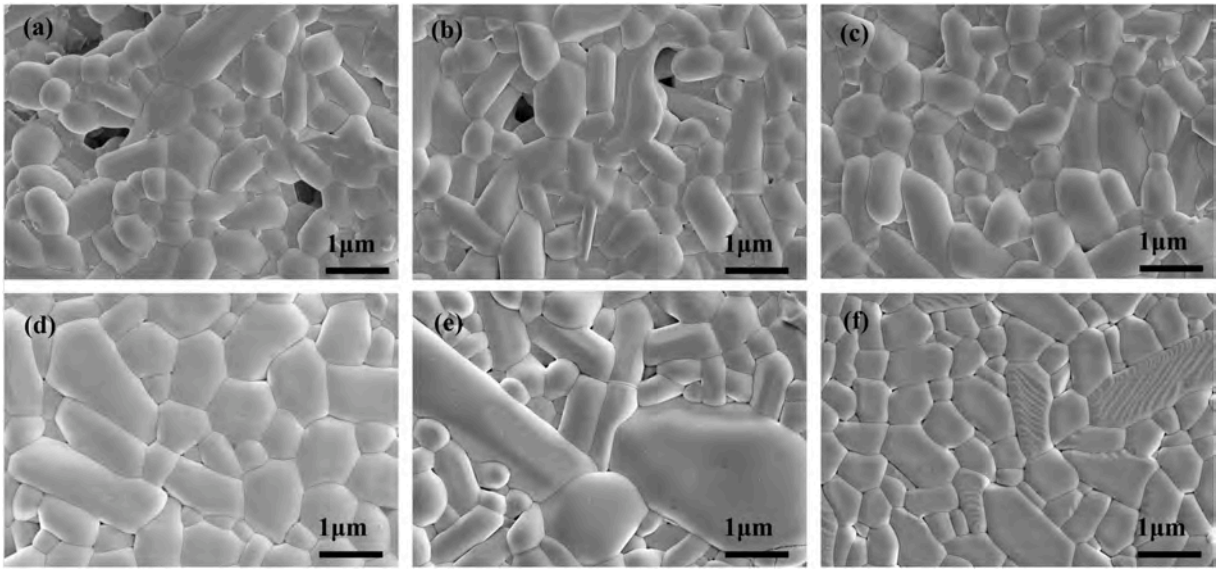

Fig. 4. SEM images of (a)–(e) $Ca_3Y_2Si_3O_{12}$ ceramics sintered at 1180 °C/6 h, 1200 °C/12 h, 1220 °C/12 h, 1240 °C/12 h, and 1260 °C/12 h and (f) $Ca_3Yb_2Si_3O_{12}$ ceramics sintered at 1260 °C/12 h.

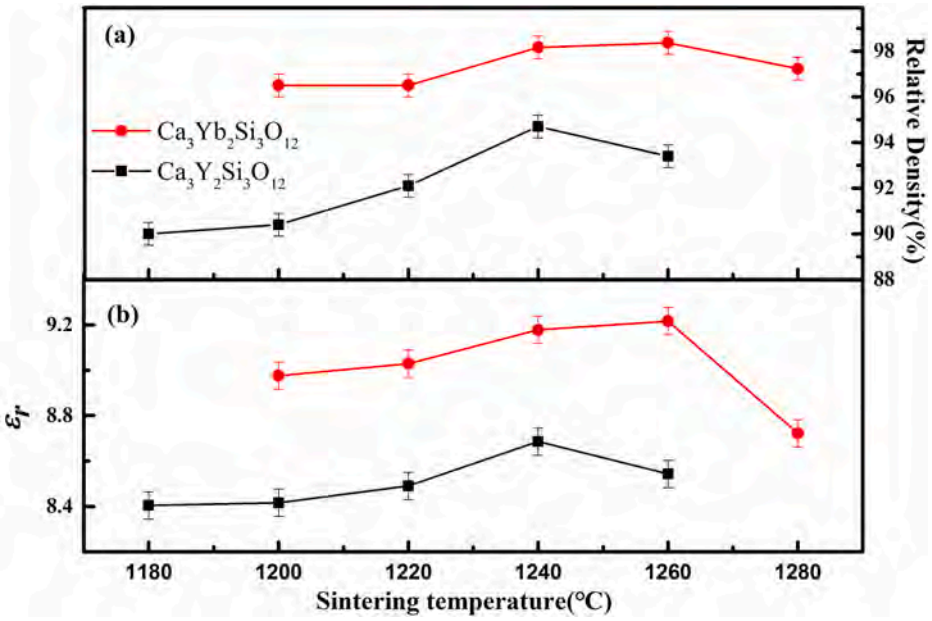

Fig. 5. Relative density, ε_r values of the $Ca_3M_2Si_3O_{12}$ (M = Yb, Y) ceramics sintered at various temperatures for 12 h.

values are 56,400 GHz for $Ca_3Yb_2Si_3O_{12}$ and 29,094 GHz for $Ca_3Y_2Si_3O_{12}$. Usually, the quality factor is closely associated with (i) the inherent losses related to the lattice vibration modes and (ii) the external factors such as secondary phase, grain morphology, grain boundaries, and porosity [22,23]. As to dense ceramics with a single-phase, the influence of the extrinsic factors can be negligible. According to Kim et al. [24,25], the relationship between $Q\times f$ and the packing fraction is the following: the lattice vibration declines as the packing fraction increases, which further causes an intrinsic loss decline. The packing fraction can be calculated by the following equation:

$$\text{packing fraction}(\%) = \frac{\text{volume of packed ions}}{\text{volume of unit cell}} \times Z \quad (5)$$

The packing fraction of $Ca_3Yb_2Si_3O_{12}$ sintered at 1260 °C was 65.35%, with the value of 62.39% for $Ca_3Y_2Si_3O_{12}$ at 1240 °C. Thus, the higher $Q\times f$ of $Ca_3Yb_2Si_3O_{12}$ than that of $Ca_3Y_2Si_3O_{12}$ could be explained by the larger packing fraction. As seen in Fig. 6, the sintering temperature had weak influence on the τ_f value and it fluctuated at −77.5 ppm/°C for $Ca_3Yb_2Si_3O_{12}$ and at −76.9 ppm/°C for $Ca_3Y_2Si_3O_{12}$.

The intrinsic dielectric properties are usually analyzed by Infrared spectroscopy. The IR reflectivity spectra of $Ca_3Yb_2Si_3O_{12}$ and $Ca_3Y_2Si_3O_{12}$ ceramics are shown in Fig. 7, which are fitted by software REFFIT according to the classic harmonic oscillator model [6]. The fitted parameters of $Ca_3Yb_2Si_3O_{12}$ ceramic are listed in Table 1 (The fitted parameters of $Ca_3Y_2Si_3O_{12}$ ceramic are listed in Table S1). The dielectric permittivity at the optical frequency are 1.94 and 1.738, and the intrinsic permittivity are 8.9 and 9.0 for $Ca_3Yb_2Si_3O_{12}$ and $Ca_3Y_2Si_3O_{12}$, respectively, which are close to the measured values of 9.2 at 13.9 GHz and 8.7 at 14.2 GHz. This indicates that the dielectric constant in the microwave band is mainly contributed by ion displacement polarization [26]. The Lorentzian function formula can be used to calculate the theoretical quality factor of $Ca_3M_2Si_3O_{12}$ (M = Yb, Y), and the dielectric

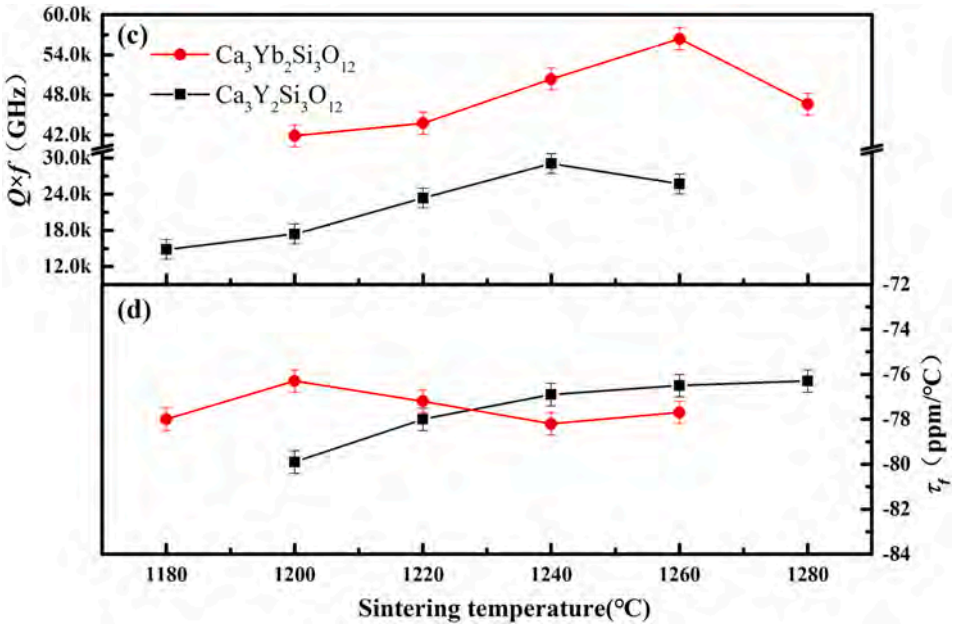

Fig. 6. The microwave dielectric properties ($Q \times f$ and τf values) of the $Ca_3M_2Si_3O_{12}$ (M = Yb, Y) ceramics sintered at various temperature for 12 h.

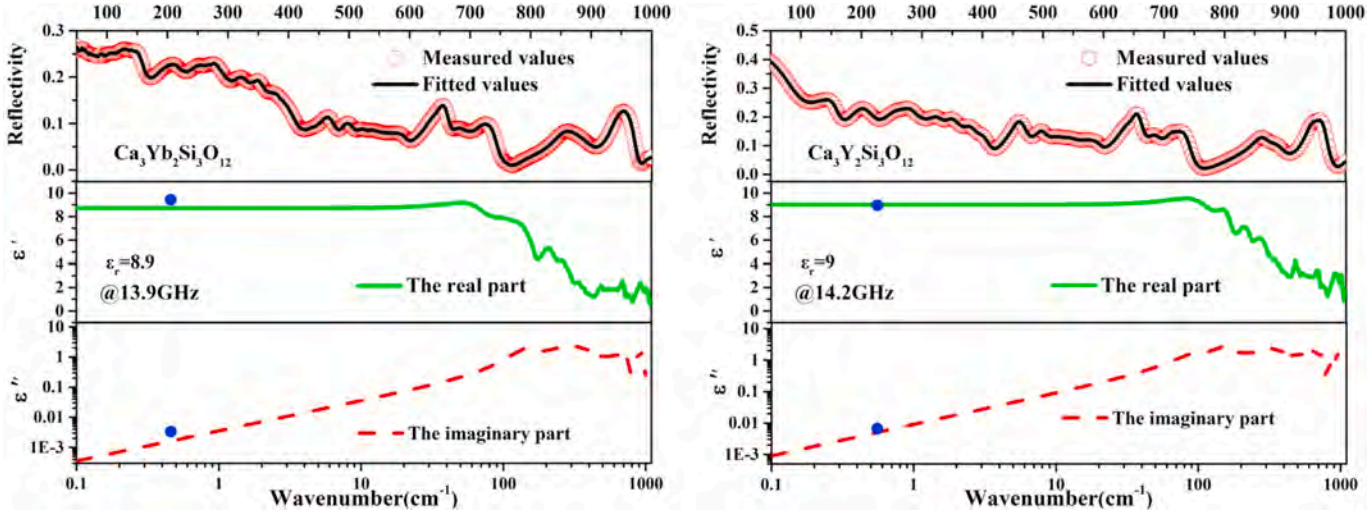

Fig. 7. The measured and fitted IR reflectivity spectra of the $Ca_3M_2Si_3O_{12}$ (M = Yb, Y) ceramic.

loss can be estimated by the following formula [27,28]:

$$\varepsilon' = \varepsilon_\infty \sum_{j=1}^{n} \frac{\omega_{pj}^2}{\omega_{oj}^2} = \varepsilon_\infty + \sum_{j=1}^{n} \Delta\varepsilon_j \tag{6}$$

$$\tan\delta = \frac{\varepsilon''}{\varepsilon'} = \omega \sum_{j=1}^{n} \frac{\Delta\varepsilon_j \gamma_j}{\omega_{oj}^2 \left(\varepsilon_\infty + \sum_{j=1}^{n} \Delta\varepsilon_j\right)} \tag{7}$$

By calculation, the theoretical $Q \times f$ value of $Ca_3Yb_2Si_3O_{12}$ is 73,815 GHz (f = 13.9 GHz) and 33,470 GHz (f = 14.2 GHz) for $Ca_3Y_2Si_3O_{12}$, which are higher than the values measured by the $TE_{01\delta}$ method. Therefore, grain size, pores and other extrinsic factors may cause the dielectric loss to increase, and the influence of the extrinsic factors can be reduced by optimizing the process to decrease the dielectric loss.

The microwave dielectrics require a close-zero τ_f to achieve the thermal stability of electronic devices. The approach of adjusting largely negative τ_f consists of adding opposite τ_f materials like $CaTiO_3$(τ_f = +800 ppm/°C) or TiO_2(τ_f = +460 ppm/°C) [29–31]. In this work, we chose to add $CaTiO_3$ to adjust τ_f by forming (1-x) $Ca_3Yb_2Si_3O_{12}$-$x$$CaTiO_3$ ceramics. Fig. 8 exhibits the XRD graphic of the (1-x) $Ca_3Yb_2Si_3O_{12}$-x-$CaTiO_3$ (x = 0.09, 0.11) ceramics sintered at 1240 °C. All the diffraction peaks of (1-x) $Ca_3Yb_2Si_3O_{12}$-$x$$CaTiO_3$ ceramics matched well with the $Ca_3Yb_2Si_3O_{12}$ and $CaTiO_3$. The top of Fig. 8 exhibits the BSE image and the EDS analysis result of x = 0.09 ceramic. The EDS analysis proved the marked darker grains belonged to $CaTiO_3$. The above evidences indicated that $Ca_3Yb_2Si_3O_{12}$ has good chemical compatibility with $CaTiO_3$. Table 2 manifests the microwave dielectric performances of (1-x) $Ca_3Yb_2Si_3O_{12}$-$x$$CaTiO_3$ ceramics. The near-zero τ_f (+2.9 ppm/°C) was acquired in 0.91$Ca_3Yb_2Si_3O_{12}$-0.09$CaTiO_3$ ceramic sintered at 1240 °C, with ε_r = 12.93, $Q \times f$ = 26,729 GHz.

4. Conclusions

Two orthorhombic silico-carnotite structured $Ca_3M_2Si_3O_{12}$ (M = Yb, Y) microwave dielectric ceramics were fabricated via high-energy ball milling and the solid-state reaction route. Dense $Ca_3Yb_2Si_3O_{12}$ and $Ca_3Y_2Si_3O_{12}$ ceramics sintered at 1260 °C and 1240 °C, respectively, presented low ε_r (9.2 and 8.7), high $Q \times f$ (56,400 GHz and 29,094 GHz),

Table 1
The phonon parameters obtained from the fitting of the infrared reflectivity spectrum of $Ca_3Yb_2Si_3O_{12}$ ceramics.

	$\omega_{oj}(cm^{-1})$	$\omega_{pj}(cm^{-1})$	γ_j	$\Delta\varepsilon_j$
1	67.606	38.202	30.597	0.667
2	99.064	63.179	57.095	0.885
3	141.2	130.23	64.429	1.4
4	154.68	52.934	23.166	0.218
5	213.15	162.74	66.606	1.01
6	253.74	114.71	44.31	0.359
7	279.92	134.38	42.74	0.31
8	299.24	60.646	33.963	0.0871
9	322.4	138.28	44.257	0.238
10	349.83	118.04	36.934	0.162
11	375.77	103.91	39.056	0.105
12	398.22	132.63	53.451	0.126
13	441	97.66	49.021	0.0698
14	465.92	117.08	35.117	0.0852
15	498.13	96.651	29.14	0.0503
16	522.07	85.707	34.897	0.0378
17	545.09	117.45	48.22	0.06
18	579.7	148.05	57.266	0.0845
19	589.25	19.432	11.704	0.00112
20	636.76	156.27	45.022	0.0848
21	654.13	118.01	25.383	0.0414
22	686.19	137.92	41.023	0.0477
23	714.9	124.4	33.285	0.0366
24	731.48	92.228	25.717	0.0181
25	859.52	214.71	55.061	0.084
26	892.41	136.81	50.693	0.0283
27	937.62	175.03	33.217	0.0415
28	954.21	104.76	24.234	0.014
29	987.1	68.269	14.903	0.00535

ε_{∞} =1.94

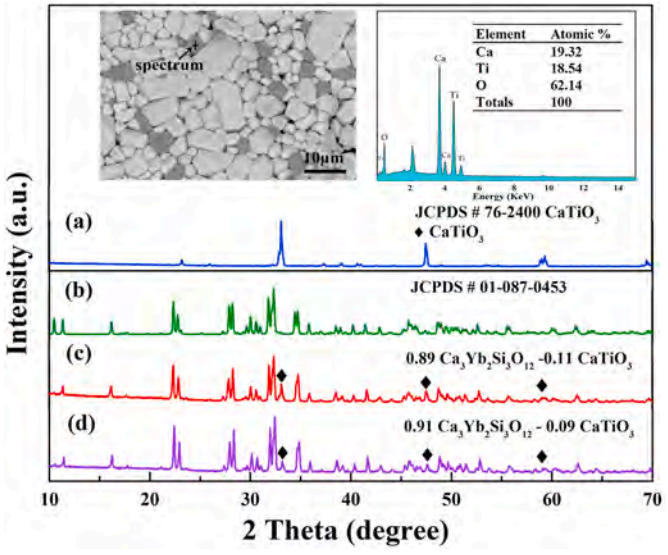

Fig. 8. XRD patterns of (1-x) $Ca_3Yb_2Si_3O_{12}$-xCaTiO$_3$ (x = 0.09, 0.11) ceramics and the BSE image with the EDS analysis result of 0.91$Ca_3Yb_2Si_3O_{12}$-0.09CaTiO$_3$.

Table 2
Microwave dielectric properties of (1−x) $Ca_3Yb_2Si_3O_{12}$-xCaTiO$_3$ composite ceramics.

x value	S.T. (°C)	ε_r	$Q \times f$ (GHz)	τ_f (ppm/°C)
0	1260	9.21	56400	−76.5
0.09	1240	12.93	26729	+2.9
0.11	1240	13.87	18193	82.79

and negative τ_f (−77.5 ppm/°C and −76.9 ppm/°C). The variation in the $Q \times f$ values of $Ca_3M_2Si_3O_{12}$ (M = Yb, Y) ceramics was highly dependent on the packing fraction. The intrinsic ε_r (8.9 and 9.0) and $Q \times f$ (73,815 GHz and 33,470 GHz) of $Ca_3Yb_2Si_3O_{12}$ and $Ca_3Y_2Si_3O_{12}$ ceramics were extrapolated based on the fitted infrared reflectivity spectra, respectively, revealing the dielectric constant in the microwave band is only contributed by ion displacement polarization. Additionally, the 0.91$Ca_3Yb_2Si_3O_{12}$-0.09$CaTiO_3$ composite ceramics were formed to adjust the largely negative τ_f successfully with ε_r = 12.93, $Q \times f$ = 26,729 GHz and τ_f = +2.9 ppm/°C.

Declaration of competing interest

The authors declare that they have no known competing financial interests or personal relationships that could have appeared to influence the work reported in this paper.

Acknowledgments

This work was supported by Natural Science Foundation of China (Nos. 21761008 and 21965009), the Natural Science Foundation of Guangxi Zhuang Autonomous Region (Nos. 2018GXNSFAA138175), and Innovation Project of Guangxi Graduate Education (YCBZ2020167 and YCBZ2020066). We are grateful to IR beamline workstation of the National Synchrotron Radiation Laboratory (NSRL) for their help with IR measurements.

Appendix A. Supplementary data

Supplementary data to this article can be found online at https://doi.org/10.1016/j.ceramint.2020.10.054.

References

[1] L.X. Pang, D. Zhou, Z. Ming Qi, Z.X. Yue, Influence of W substitution on crystal structure, phase evolution and microwave dielectric properties of ($Na_{0.5}Bi_{0.5}$)MoO_4 ceramics with low sintering temperature, Sci. Rep. 7 (2017) 3201.
[2] D. Zhou, L.X. Pang, D.W. Wang, C. Li, B.B. Jin, I.M. Reaney, High permittivity and low loss microwave dielectrics suitable for 5G resonators and low temperature co-fired ceramic architecture, J. Mater. Chem. C 5 (2017) 10094–10098.
[3] M.T. Sebastian, R. Ubic, H. Jantunen, Low-loss dielectric ceramic materials and their properties, Ceram. Int. 60 (7) (2017) 392–412.
[4] Y. Tang, Z.W. Zhang, J. Li, M.Y. Xu, Y.F. Zhai, L. Duan, C.X. Su, L.J. Liu, Y.H. Sun, L. Fang, $A_3Y_2Ge_3O_{12}$ (A = Ca, Mg): two novel microwave dielectric ceramics with contrasting τ_f and Q×f, J. Eur. Ceram. Soc. 40 (12) (2020) 3989–3995.
[5] H Zhou, C Lu, S Li, J.J. Deng, K.G. Wang. Phase composition, sintering behavior and mirowave dielectric properties of novel high Q $Ca_3Al_2(GeO_4)_3$ ceramic. Mater. Lett. 263.
[6] J. Chen, Y. Tang, H. Xiang, L. Fang, H. Porwal, C. Li, Microwave dielectric properties and infrared reflectivity spectra analysis of two novel low-firing $AgCa_2B_2V_3O_{12}$ (B = Mg, Zn) ceramics with garnet structure, J. Eur. Ceram. Soc. 38 (2018) 4670–4676.
[7] H. Yamane, T. Nagasawa, M. Shimada, T. Endo, $Ca_3Y_2(SiO_4)_3$, Acta Crystallogr. C53 (1997) 13.
[8] D.L. Poerschke, T. L Barth, O. Fabrichnaya, C.G. Levi, Phase equilibria and crystal chemistry in the calcia–silica–yttria system, J. Eur. Ceram. Soc. 36 (7) (2016) 1743–1754.
[9] F. Piccinelli, A. Speghini, G. Mariotto, F. Piccinelli, A. Speghini, G. Mariotto, L. Bovo, M. Bettinelli, Visible luminescence of lanthanide ions in $Ca_3Sc_2Si_3O_{12}$ and $Ca_3Y_2Si_3O_{12}$, J. Rare Earths 27 (4) (2009) 555–559.
[10] A. Dobrowolska, E. Zych, Spectroscopic characterization of $Ca_3Y_2Si_3O_{12}$: Eu^{2+}, Eu^{3+} powders in VUV-UV–vis region, J. Phys. Chem. C 116 (48) (2012) 25493–25503.
[11] B. V Rao, Y.T. Nien, W.S. Hwang, I.G. Chen, An investigation on luminescence and energy transfer of Ce^{3+} and Tb^{3+} in $Ca_3Y_2Si_3O_{12}$ phosphors, J. Electrochem. Soc. 156 (11) (2009) 338–341.
[12] V.R. Bandi, B.K. Grandhe, K. Jang, H.S. Lee, S.S. Yi, J.H. Jeong, Citric based sol-gel synthesis and photoluminescence properties of un-doped and Sm^{3+} doped $Ca_3Y_2Si_3O_{12}$ phosphors, Ceram. Int. 37 (6) (2011) 2001–2005.
[13] L. Cheng, P. Liu, X.M. Chen, W. Niu, G. Yao, C. Liu, X. Zhao, Q. Liu, H. Zhang, Fabrication of nanopowders by high energy ball milling and low temperature sintering of Mg_2SiO_4 microwave dielectrics, J. Alloys Compd. 513 (2012) 373–377.
[14] K.X. Song, X.M. Chen, X.C. Fan, Effects of Mg/Si ratio on microwave dielectric characteristics of forsterite ceramics, J. Am. Ceram. Soc. 90 (6) (2007) 1808–1811.
[15] S.B. Kim, S.J. Kim, C.H. Kim, W.S. Kim, K.W. Park, Nanostructure cathode materials prepared by high-energy ball milling method, Mater. Lett. 65 (2011) 3313–3316.

[16] R.D. Shannon, C.T. Prewitt, Acta Crystallogr. B 25 (1969) 925–946.
[17] J. Guo, D. Zhou, L. Wang, H. Wang, T. Shao, Z.M. Qi, X. Yao, Infrared spectra, Raman spectra, microwave dielectric properties and simulation for effective permittivity of temperature stable ceramics $AMoO_4$ –TiO_2 (A = Ca, Sr), Dalton Trans. 42 (2013) 1483–1491.
[18] D. Zhou, W.B. Li, J. Guo, L.X. Pang, Z.M. Qi, T. Shao, H.D. Xie, Z.X. Yue, X. Yao, Structure, phase evolution, and microwave dielectric properties of $(Ag_{0.5}Bi_{0.5})(Mo_{0.5}W_{0.5})O_4$ ceramic with ultralow sintering temperature, Inorg. Chem. 53 (2014) 5712–5716.
[19] X. Tong, Q.L. Zhang, H. Yang, J.L. Zou, Low-temperature firing and microwave dielectric properties of Ca $[(Li_{0.33}Nb_{0.67})\ 0.9Ti_{0.1}]\ O_3$–$\delta$ ceramics with LiF addition, Mater. Lett. 59 (2005) 3252–3255.
[20] S.H. Yoon, D.W. Kim, S.Y. Cho, K. Hong, Investigation of the relations between structure and microwave dielectric properties of divalent metal tungstate compounds, J. Eur. Ceram. Soc. 26 (2006) 2051–2054.
[21] R.D. Shannon, Dielectric polarizabilities of ions in oxides and fluorides, J. Appl. Phys. 73 (1993) 348–366.
[22] Z.W. Zhang, L. Fang, H.C. Xiang, C.C. Li, Y. Tang, M.Y. Xu, Jantunen, H. Structural, Infrared reflectivity spectra and microwave dielectric properties of the $Li_7Ti_3O_9F$ ceramic, Ceram. Int. 45 (2019) 10163–10169.
[23] J. Guo, D. Zhou, L. Wang, H. Wang, S. Tao, Z.M. Qi, Y. Xi, Infrared spectra, Raman spectra, microwave dielectric properties and simulation for effective permittivity of temperature stable ceramics $AMoO_4$–TiO_2 (A = Ca, Sr), Dalton Trans. 42 (5) (2013) 1483–1491.
[24] H.C. Xiang, C.C. Li, H. Jantunen, L. Fang, A. Hill, Ultralow loss $CaMgGeO_4$ microwave dielectric ceramic and its chemical compatibility with silver electrodes for low-temperature cofired ceramic applications, ACS SUSTAIN CHEM ENG 6 (5) (2018) 6458–6466.
[25] E.S. Kim, B.S. Chun, R. Freer, R.J. Cernik, Effects of packing fraction and bond valence on microwave dielectric properties of $A^{2+}B^{6+}O_4$ (A^{2+}: Ca, Pb, Ba; B^{6+}: Mo, W) Ceramics, J. Eur. Ceram. Soc. 30 (2010) 1731–1736.
[26] Y.K. Yang, Y.Z. Wang, J.J. Zheng, N. Dai, R.H. Li, H.T. Wu, B. Wu, Microwave dielectric properties of ultra-low loss $Li_2Mg_4Zr_{0.\ 95}\ (Mg_{1/3}Ta_{2/3})_{\ 0.05}\ O_7$ ceramics sintered at low temperature by LiF addition, J. Alloys Compd. 786 (2019) 867–872.
[27] J. Guo, D. Zhou, L. Y Li, T. Shao, H. Wang, Structure–property relationships of novel microwave dielectric ceramics with low sintering temperatures: $(Na_{0.5x}Bi_{0.5x}Ca_{1-x})\ MoO_4$, Dalton Trans. 43 (31) (2014) 11888–11896.
[28] K. Wakino, M. Murata, H. Tamura, Far infrared reflection spectra of Ba (Zn, Ta) O_3-$BaZrO_3$ dielectric resonator material, J. Am. Ceram. Soc. 69 (1) (1986) 34–37.
[29] A. Ullah, H.X. Liu, H. Hao, J. Iqbal, Z.H. Yao, M.H. Cao, Influence of TiO_2 additive on sintering temperature and microwave dielectric properties of $Mg_{0.90}Ni_{0.1}SiO_3$ ceramics, J. Eur. Ceram. Soc. 37 (2017) 3045–3049.
[30] H.R. Zheng, S.H. Yu, L.X. Li, X.S. Lyu, Z. Sun, S.L. Chen, Crystal structure, mixture behavior, and microwave dielectric properties of novel temperature stable (1-x) $MgMoO_4$ -$xTiO_2$ composite ceramics, J. Eur. Ceram. Soc. 37 (2017) 4661–4665.
[31] X.C. Wang, W. Lei, R. Ang, W.Z. Lu, $ZnAl_2O_4$ -TiO_2 -$SrAl_2Si_2O_8$ low-permittivity microwave dielectric ceramics, Ceram. Int. 39 (2013) 1707–1710.